Computer Methods and Programs in Biomedicine Update 1 (2021) 100027

Contents lists available at ScienceDirect

Computer Methods and Programs in Biomedicine Update

journal homepage: www.sciencedirect.com/journal/computer-methods-and-programs-in-biomedicine-update

A new method for accurate detection of movement intention from single channel EEG for online BCI

Maryam Mahmoodi [a,b,1,*], Bahador Makkiabadi [a,b,1,*], Mehran Mahmoudi [c], Saeid Sanei [d]

[a] Department of Medical Physics and Biomedical Engineering, School of Medicine, Tehran University of Medical Sciences (TUMS), Tehran, Iran
[b] Research Center for Biomedical Technology and Robotics (RCBTR) of Advanced Medical Technologies and Equipment Institute (AMTEI), Tehran University of Medical Sciences, Tehran, Iran
[c] Department of Mechanical Engineering, University of Tehran, Tehran, Iran
[d] School of Science and Technology, Nottingham Trent University, Nottingham, U.K

ARTICLE INFO

Keywords:
BCI
Convex optimization
EEG
Nonlinear
Readiness potential (RP)
Teager-Kaiser energy operator (TEO)

ABSTRACT

Low frequency readiness potential (RP) is elicited in electroencephalograms (EEGs) as one intends to perform an imagery (IMI) or real movement (RMI). While in most brain-computer-interface (BCI) applications the challenge is to classify RPs of different limbs from the given EEG trials, the objective of this study is fast and automatic detection of RPs from the entire single channel EEG signal. The proposed algorithm has two threshold blocks based on the nonlinear Teager-Kaiser energy operator (TEO) in the first block and the morphological properties of the RP waveform as constraints in the second block. The performance is strongly influenced by the abrupt energy changes due to transients and artefacts. As the major contribution, the proposed nonlinear convex optimization algorithm enables separation of transients from low frequency components by providing a fast thresholding mechanism. Application of the proposed method to Physionet RMI dataset, BCI competitionIV-1 IMI dataset and our own left hand movement datasets of healthy subjects led to true positive rates (TPRs) of 76.5±8.27%, 83.85±11.4%, and 81.1±5.23%, number of FPs/min of 2.4±1.07, 1.4±0.7, and 1.6±0.69 and accuracy rates of 85.4±3.83%, 90±3.56%, and 91.2±2.04%. Movement onset detection latency from our automatic RP detector was -384.9±296.5 ms.

As a conclusion, the proposed method outperforms state-of-the-art techniques using as low as single channel EEG making it suitable for real-time neuro-rehabilitation of paralyzed subjects suffering from stroke.

Introduction

Since the detection of bereitschafts potential (BP) or readiness potential (RP) in 1964 by Kornhuber and Deecke [1-3], it has been proven that RP is initiated as early as 2 s before starting a voluntary movement. Its low amplitude oscillatory changes continues to approximately 400 ms before the movement onset and proceeds as a low frequency negative slope (NS) component which is followed by a positive slope and oscillations after the movement onset. The time for the end point of the NS component is the movement onset to trigger a real movement. RP may be considered as a slow wave in delta frequency [4]. Besides real movement intention (RMI), RP is also evoked by imagery movement intention (IMI) [5,6]. It's a cortical potential produced by motor cortex neurons which is evident in the EEG over central electrodes.

Brain-computer-interface (BCI) systems with the aim of neuro-modulation of cortico-muscular interactions follow two objectives: training subjects to improve their motor potentials (MPs) by applying a cue to imagine a specific limb movement and a duration for rest [7]. At last a scoring system is used to feedback how successful they are in producing their RPs. On the other hand, one aims to control a prosthetic limb or an attached motor unit [8,9] from their own RPs. For the latter purpose we need smart devices [10,11] to early detect the RMIs to facilitate real-life activities for paralyzed subjects. The latter one is the main objective of this paper, i.e., developing a fast and accurate method for early detection of RPs with the future purpose of real-time implementation. Our proposed method also meets the first objective, i.e.,

* Corresponding authors at: Department of Medical Physics and Biomedical Engineering, School of Medicine, Tehran University of Medical Sciences (TUMS), Tehran, Iran.
E-mail addresses: mahmoodi-m@razi.tums.ac.ir (M. Mahmoodi), b-makkiabadi@tums.ac.ir (B. Makkiabadi).
[1] The first authorship is joint between Maryam Mahmoodi and Bahador Makkiabadi.

https://doi.org/10.1016/j.cmpbup.2021.100027
Received 30 November 2020; Received in revised form 25 July 2021; Accepted 18 August 2021
Available online 20 August 2021

detection of the RPs due to IMIs for neurofeedback scoring devices.

Till now, many works have been carried out for early detection of RP, with the use of single or multiple channel EEG. Nguyen et al. [9] detected braking intention with 8- channel EEG during simulated driving. Feeding artificial neural network (ANN) with autoregressive (AR) model-based features; they achieved an average sensitivity of 88.4%, an average accuracy of 91% and average −600 ms movement onset detection latency. In [7] the movement intention was detected from single trial EEGs of 8 healthy subjects with an average sensitivity of 75% and an average detection latency of −206 ms before the movement onset. They applied template matching to laplacian spatial filtered EEG. In [12] it has been shown that the spectral features fed into a linear discriminant classifier lead to an average 5.5% detection error and 93% sensitivity which is much better than using template matching (average 28.9% detection error and 82% sensitivity) [13]. The authors in [14,15] proposed a constrained blind source extraction method for detection of RPs from non-invasive EEG of RMIs. In [16], the authors applied a template matching algorithm to single channel EEG for detection of movement intention. They achieved an average TPR of 78% and an average movement onset detection latency of −150 ms. Mahmoodi et al. [17] proposed a robust beamformer to extract RP from neuron activities on primary motor cortex from 64-channel EEG and detected the movement intentions 512 ms in average before the movement onsets with 28% false positive rate (FPR) and 77% sensitivity. Beamforming can be used as a denoising technique to reconstruct specific source(s) on predefined location(s) in space from their mixture [18] and has been implemented on a single channel field programmable gate array (FPGA) board in [19,20] for telecommunication purposes. For medical purposes, e.g., EEG beamforming for brain source reconstruction, at least 64 channels [18] are needed for sufficient spatial resolution, which makes it complicated to implement for neuromodulation purposes. Unlike our previous work [17], we aim to propose a fast and highly accurate method for detection of movement intention from a single channel EEG in this study to enable low cost and easy implementation in future neuromodulation applications. Solnik et al. [21] applied the nonlinear Teager-Kaiser energy operator (TEO) to the EMG signals resulting in the TEO-signal which could continuously track the energy changes of the EMG signal. They showed that applying a threshold to the TEO-signal helps detection of movement onset with an average latency of −229 ms which is earlier than latency of onset detection by directly applying a threshold to the EMG signal (−40 ms). In this paper, we use two threshold blocks for automatic RP detection. The nonlinear TEO on EEG signal resulting in the TEO-signal is used in the first threshold block and RPs are detected when their negative ramps make increasing energy changes to the TEO-signal. The second threshold block gets each segment of the EEG signal detected from the first threshold block as input and next compares its properties in terms of duration and slope with predefined morphological properties of a true RP waveform as the limiting constraints for final decision. The second threshold block effectively reduces false detections from the first block. Unlike template matching and machine learning based methods, our method does not need any data splitting into trials or data training. The best performance of our RP detector is determined from the receiver-operating-characteristic (ROC) curve through which the optimum threshold for the first threshold block, TEO-signal, is also determined. Our proposed RP detector is strongly influenced by the sudden energy changes of the signal due to transients and artefacts. Hence, an effective nonlinear threshold-based transient suppression method based on a convex optimization model is applied to the EEG signal in the EEG preprocessing stage before RP detection. The EEG also goes to a threshold block for fast detection and immediate suppression of the high amplitude eye blinking artefacts. Our proposed RP detector, evaluated on three datasets, is able to detect RPs (IMIs or RMIs) continuously over time. From [1, 2], we know that the neural activity of RP on primary motor cortex projects better on central region electrodes, contra-lateral to the movement direction. As determining the origin of movement,

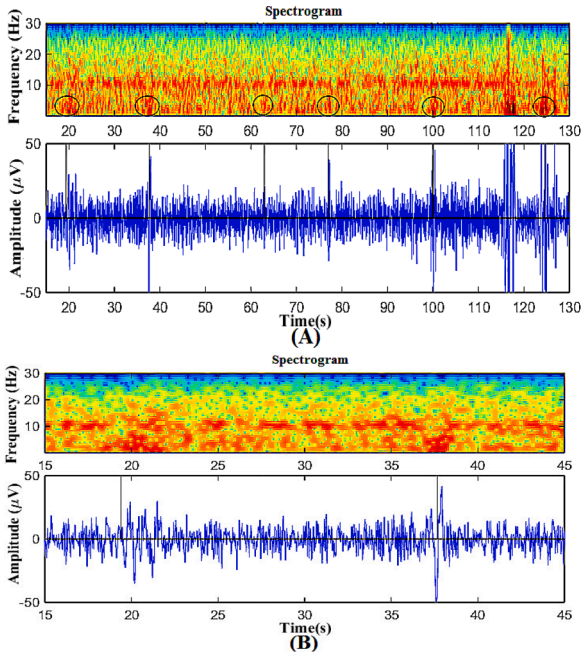

Fig. 1. (**A**) EEG of left hand movement and EEG spectrogram acquired with STFT on 400 ms windows with 99% overlap and the sampling frequency (fs) of 256 Hz. Spectrogram, implemented on 1–30 Hz bandpass filtered EEG signal, shows hotspots in frequencies less than 10 Hz (0–5 Hz) around the movement onsets (black vertical bars on the signal). (**B**) Zoomed signal and corresponding spectrogram of the top figure in 15–45 s for better realization of low frequency energy changes around the movement onsets.

corresponding to each detected RP, is not the purpose of this study, and with a glance to low cost online implementation of our RP detector in future, the best position to pick up the RPs for both sides is over the midline motor area, i.e. Cz.

We know that we would need more electrodes for determining the origin of movement. We show that it is possible to have a fast and highly accurate RP detector from a single channel EEG.

Methods

Preprocessing

The EEG preprocessing involves transient removal, EOG blinking artefact rejection and lowpass filtering. First, using short-time Fourier transform (STFT) based time-frequency analysis, the EEG spectrogram is plotted. Each signal segment is bandpass filtered over 1–30 Hz using a 20th order linear phase FIR filter. In Fig. 1, the RPs are marked by black vertical bars on the signal at the starting times of voluntary left-hand movements by pressing a soft push button in hand. Although, the push button was soft enough for the subjects that they didn't need much effort, the accuracy of movement onset was also validated by the EMG signal. In an offline processing, we first find EMG peaks and next find the nearest time corresponding to 10% of each peak amplitude as movement onset. Then, we validate the markers from push button with markers from EMG. Moreover, our subjects were already asked and trained to press buttons exactly at the time of their movement intention. From Fig. 1, the RPs generate low frequency (0–5 Hz) hotspots on the spectrogram color-map. There are also energy changes in rest durations due to high frequency transients or myogenic artefacts which are inevitable in non-stationary artefact contaminated signals.

Transients on the EEG signal are suppressed by applying a nonlinear method, called total variation denoising (TVD) [22,23]. Unlike conventional lowpass filter, TVD filter is defined by a nonlinear optimization approach for noise suppression whereas preserving low frequency

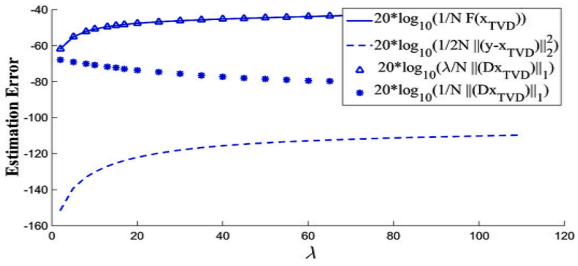

Fig. 2. Output estimation Error curves with respect to λ (defined in (5)).

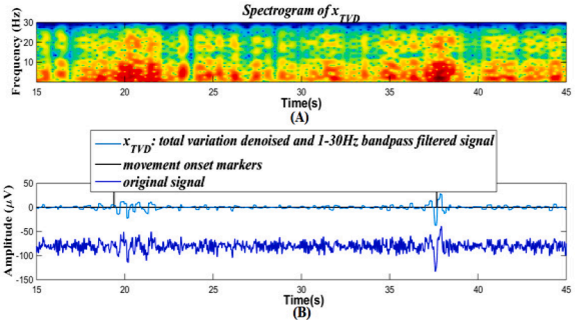

Fig. 3. (**A**) Spectrogram of $\boldsymbol{x}_{TVD}$, i.e., TVD and 1–30 Hz 20th order FIR bandpass filtered signal of Fig. 1(B). (**B**) $\boldsymbol{x}_{TVD}$ (light blue), acquired with smoothing parameter λ=70 and movement onset markers (black vertical bars) and original signal (dark blue). Suppressing EEG transients, TVD makes RPs visually more dominant on the EEG and spectrogram. Signals of Fig. 1(B) and Fig. 3 are intentionally made the same to comprehend the TVD effect.

sharp edges and shape of the underlying signal [22-24,25-27]. Let's assume $\boldsymbol{y}$ is a noisy signal as:

$$\boldsymbol{y}(n) = \boldsymbol{x}(n) + \boldsymbol{w}(n),\ n = 0,\ \ldots,\ \mathrm{N}-1 \tag{1}$$

where $\boldsymbol{x}$ is (an approximately) piecewise constant signal with a sparse derivative and $\boldsymbol{w}$ is white Gaussian noise. The total variation *(TV)* of the signal $\boldsymbol{x}(n)$ with N points is defined as L_1-norm ($\|\ .\ \|_1$) of its derivative [22,23]:

$$TV(\boldsymbol{x}) = \|\ \boldsymbol{Dx}\ \|_1 = \sum_{n=1}^{N-1} |\boldsymbol{x}(n) - \boldsymbol{x}(n-1)| \tag{2}$$

where $|.|$ denotes the absolute value. TVD means to estimate the signal $\boldsymbol{x}$ from the noisy signal, $\boldsymbol{y}$, by minimizing the following nonlinear convex objective function $F(\boldsymbol{x})$ [23]:

$$\underset{\boldsymbol{x}}{arg\ min}\left\{ F(\boldsymbol{x}) = \frac{1}{2}\sum_{n=0}^{N-1} |\boldsymbol{y}(n) - \boldsymbol{x}(n)|^2 + \lambda \|\ \boldsymbol{Dx}\ \|_1 \right\} \tag{3}$$

where λ is the regularization and smoothing factor which controls the degree of smoothness in $\boldsymbol{x}$. The first statement after equation equals power 2 of *L_2-norm* ($\|\ .\ \|_2^2$). So, (3) can be rewritten as the following convex optimization equation:

$$\underset{x \epsilon R^N}{arg\ min}\left\{ F(\boldsymbol{x}) = \frac{1}{2}\|\ \boldsymbol{y} - \boldsymbol{x}\ \|_2^2 + \lambda \|\ \boldsymbol{Dx}\ \|_1 \right\} \tag{4}$$

A direct noniterative threshold-based solution was proposed in [22] and released with a C code implementation. This method is suitable for online processing of the signal, since the incoming jumps in the signal amplitude are detected and suppressed one after the other. The reader is referred to the Appendix A and [22] for details on the denoising algorithm. We call the output N-*point* denoised signal as $\boldsymbol{x}_{TVD}$. The output normalized error as defined in (4) is only dependent on λ and is defined

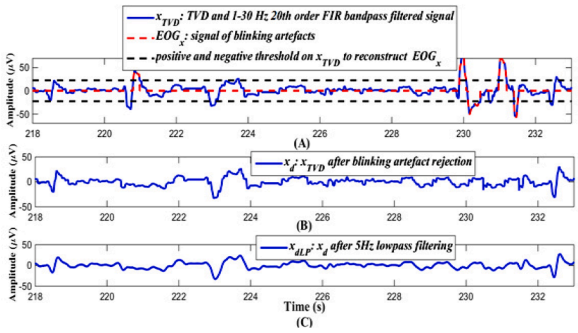

Fig. 4. (**A**) $\boldsymbol{x}_{TVD}$ (blue) and $\boldsymbol{EOG}_x$ (red), signal of triangular eye blinking artefacts. $\boldsymbol{EOG}_x$ is acquired by applying an appropriate data-driven threshold ((6)) to absolute value of $\boldsymbol{x}_{TVD}$. Blinkings are those segments with absolute values exceeding the threshold (positive/negative black dashed lines) and 45 μV. (**B**) $\boldsymbol{x}_d$, denoised signal after artefact rejection by replacing 0.5 s around mid-point of each artefact contaminated segment with its previous clean part. (**C**) $\boldsymbol{x}_{dLP}$, i.e., $\boldsymbol{x}_d$ after applying a 5 Hz 4th order butterworth lowpass filter.

in decibel (dB) by:

$$Error\ = 20\log_{10}\left(\frac{1}{\mathrm{N}}F(\boldsymbol{x}_{TVD})\right) \tag{5}$$

Calculating (5) by each part in (4) with respect to λ gives the estimation error curves for the noniterative TVD method. From Fig. 2, a lower λ minimizes the errors, but increasing λ lowers the variations in $\boldsymbol{x}_{TVD}$ ($\|\ \boldsymbol{Dx}_{TVD}\|_1$) whereas slowly increases the errors to a steady constant. The smoothing parameter $\lambda = 70$ was selected in our study since giving more smoothness to $\boldsymbol{x}_{TVD}$ empirically facilitates detection of the low frequency RPs on $\boldsymbol{x}_{TVD}$ and the spectrogram as shown in Fig. 3. Hence, it increases the accuracy of our energy-based RP detection algorithm. TVD implementation time in MATLAB R2014b, a corei5 system with 4GB RAM and 2 GHz CPU speed is 0.01 s for a 5-minute signal. The $\boldsymbol{x}_{TVD}$ signal is then filtered by a 1–30 Hz 20th order FIR bandpass filter (Fig. 3). Next, each 2 s $\boldsymbol{x}_{TVD}$ segment with amplitude exceeding 110 μV (generally any threshold suitable by visual inspection) is replaced with zero-mean random numbers for myogenic artefact rejection. This method is discussed in the Appendix B.

Since TVD saves sharp low frequency peaks like eye blinking artefacts, one other denoising step is needed to remove high amplitude eye blinking (EOG) artefacts. Blinking artefacts produce low frequency hotspots in the frequency range of movement hotspots and may lead to false positives (FPs) in automatic RP detection. We empirically (by visual inspection) found an appropriate adaptive threshold for detection of blinking waveforms on the $\boldsymbol{x}_{TVD}$ signal as:

$$Threshold = \frac{3}{N}\|\ \boldsymbol{x}_{TVD}\ \|_1 \tag{6}$$

where N is the number of samples of $\boldsymbol{x}_{TVD}$. Absolute values of $\boldsymbol{x}_{TVD}$ which are greater than both *Threshold* and 45 μV are defined as the eye blinking segments. $\boldsymbol{EOG}_x$, the red-colored signal in Fig. 4(A), is the signal of blinking artefact. It has the same length as $\boldsymbol{x}_{TVD}$ with amplitudes equal to the $\boldsymbol{x}_{TVD}$ amplitudes at times during which absolute values of $\boldsymbol{x}_{TVD}$ crosses both the Threshold and 45 μV and zeros elsewhere, hence $\boldsymbol{EOG}_x$ tracks blinking triangular waveforms on $\boldsymbol{x}_{TVD}$. For blinking rejection, a duration of 0.5 s before and 0.5 s after the mid-point of each triangular waveform on $\boldsymbol{x}_{TVD}$ (as the blinkings take duration of almost 1 s) is replaced with previous clean segment of $\boldsymbol{x}_{TVD}$. Suppressing EOG artefacts in this way avoids discontinuities in the denoised signal. We refuted to use this method for rejection of myogenic artefact since the duration of muscular artefact is variable and it usually lasts longer than blinking, wich has almost fixed duration and certain triangular pattern. This shows the need for wider clean segments for replacement which are, of course, more probable to contain RPs. Hence, the replacement with last

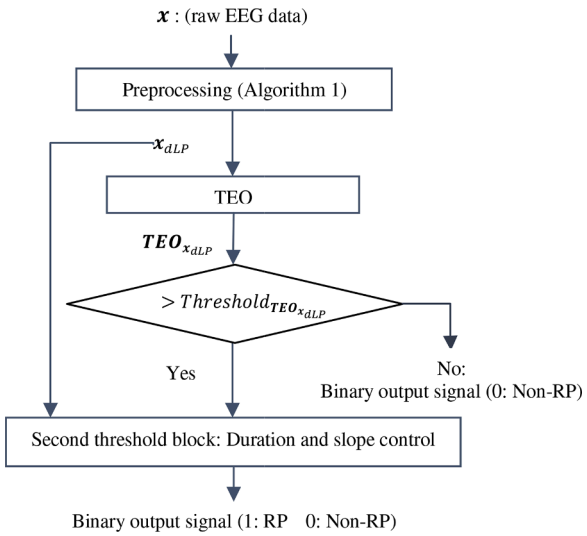

Fig. 5. Block diagram of the RP detection algorithm.

segments for this kind of artefact may lead to False RP detections, and that's why we preferred replacing with zero-mean random numbers for myogenic rejection. Denoised signal, x_d, is shown in Fig. 4(B). For the last preprocessing step, a 5 Hz 4th order butterworth lowpass filter is applied to x_d, resulting in the x_{dLP} (Fig. 4(C)), since energy changes around movement onsets are tracked in this frequency range. Preprocessing blocks are described in Algorithm 1.

RP detection algorithm

The proposed method for RP detection contains two threshold blocks. Fig. 5 briefly shows the RP detection block diagram. The first threshold block detects RPs based on energy tracking of preprocessed signal, x_{dLP}, by the nonlinear TEO [28]. Continuous and discrete TEO of x_{dLP} at continuous and discrete times, t and n, are defined by [28]:

$$TEO_{x_{dLP}}(t) = \dot{x}^2_{dLP}(t) - x_{dLP}(t)\,\ddot{x}_{dLP}(t), \tag{7}$$

$$TEO_{x_{dLP}}(n) = \frac{x_{dLP}{}^2(n) - x_{dLP}(n-\Delta n)\,x_{dLP}(n+\Delta n)}{(\Delta n)^2} \tag{8}$$

where . and .. refer to first and second order derivatives. Considering each signal amplitude in discrete time as one sample, Δn is the sample interval which is 1 in discrete time. TEO is applied to the preprocessed signal, x_{dLP}, sample by sample and results in an energy signal ($TEO_{x_{dLP}}$) with the same length as x_{dLP}. $TEO_{x_{dLP}}$, as shown in Fig. 6, peaks around RPs. Hence, applying a threshold to $TEO_{x_{dLP}}$ is the solution for RP detection. Threshold is defined by:

$$Threshold_{TEO_{x_{dLP}}} = avg\left(TEO_{x_{dLP}}\right) - c\;\delta\left(TEO_{x_{dLP}}\right) \tag{9}$$

where *avg* is the average value operator and δ is the standard deviation operator. The parameter "c" is a variable coefficient which determines the performance of the final RP detection in terms of TPR and number of FPs/min. This will be discussed later. The time segments in which $TEO_{x_{dLP}}$ rises, crosses the predefined $Threshold_{TEO_{x_{dLP}}}$, and remains above the threshold are defined on x_{dLP} as segments of primarily detected RPs. The second threshold block gets those segments on x_{dLP}, primarily detected from the first threshold block, and rejects false detections (FPs) by comparing the morphological properties of the detected RPs with the general morphological properties of a true RP waveform for final decision. The general morphological properties, as shown in Fig. 6(A) are defined in terms of duration, slope1 and slope2 from RPs around movement onsets in duration of rising the $TEO_{x_{dLP}}$. The two measurements slope1 and slope2 for each EEG segment are defined by:

$$\text{slope1} = \text{amp}_{\text{start}} - \text{amp}_{\text{min}};\ \text{slope2} = \text{amp}_{\text{end}} - \text{amp}_{\text{min}} \tag{10}$$

where $\text{amp}_{\text{start}}$, amp_{min} and amp_{end} are defined for each segment on x_{dLP} as the amplitudes of starting point, minimum amplitude point and the end point. Calculating these parameters around movement onsets (Fig. 6 (A)), averaged over all 10 subjects in our experiment of voluntary left hand movements, give the general morphological properties of a RP waveform. Since we don't want to lose RPs, it is important to know which minimum duration is acceptable for a segment length to be an RP. First, the segment lengths were detected by thresholding the $TEO_{x_{dLP}}$ around movement onset markers.

Next, minimum RP duration for each subject was detected. Finally, average over all minimum durations of our subjects' RPs was concluded to be 300 ms as the duration constraint. The average slopes are in the following range:

$$5\,\mu\text{V} < \text{slope1} < 45\mu\text{V};\ 5\,\mu\text{V} < \text{slope2} < 45\,\mu\text{V}. \tag{11}$$

Each primarily detected segment on x_{dLP} with duration more than 300 ms and slopes in the determined range of (11) is detected as a final RP segment (Fig. 6(B)). The binary output signal is 1 in time samples of detected RPs and 0 elsewhere. Our RP detector procedure is applied to each 10 s non-overlapping signal length as it is the empirical duration used by clinicians in which EEG can be considered statioary. Using "slope" instead of "amplitude difference" may be misleading since (10) is exactly the amplitude difference. But why we didn't define the slope as the amplitude difference divided by duration? This is because we didn't put limitation on the upper boundary of duration. We had tried it at first with upper boundaries on durations but the result of RP detection was

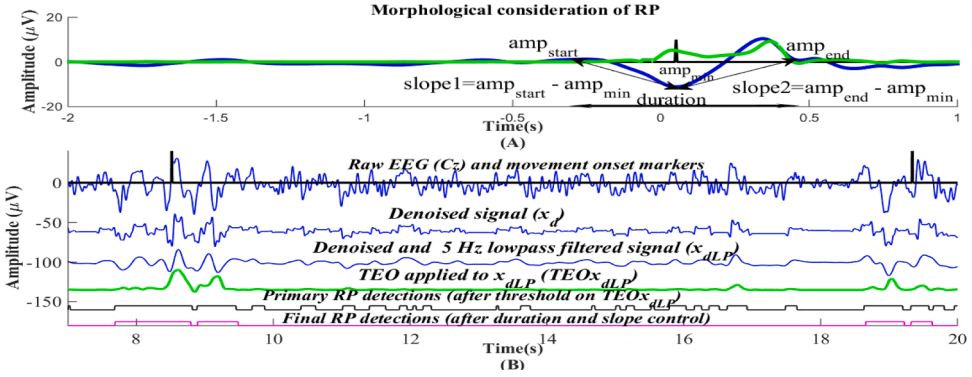

Fig. 6. (**A**) Morphological consideration of RP waveform in terms of duration and slopes (slope1 and slope2) in the duration of rising $TEO_{x_{dLP}}$ (in green) around movement onset (black bar). Average durations and slopes from all subjects in our study give the general morphological properties (in (11)) of RP waveform. (**B**) RP detection steps; Automatic RP detection (pink rectangles) as a binary signal determined by threshold on $TEO_{x_{dLP}}$ and morphological constraints (**A**) on x_{dLP}.

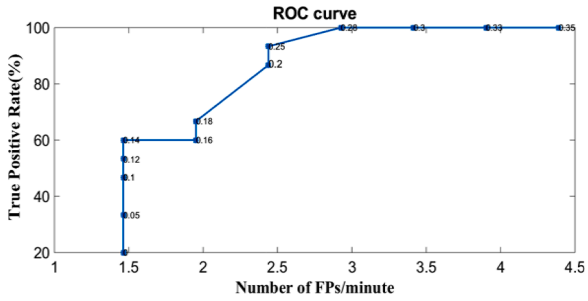

Fig. 7. *The ROC curve from the EEG signal of one subject obtained by changing coefficient "c" (in (9)) in the RP detection algorithm. The knee point of ROC curve determines the appropriate "c" which results in the maximum TPR* vs. *minimum average number of FPs/*min.

not sensitive and rejected many true RPs. So, we preferred just a lower bound for high performance.

From Fig. 6(B), in a real non stationary EEG data, we may have some intra and inter-subject variabilities in the starting point of negative ramp. Although, the RP negative ramp component is not probable to start earlier than 1 s, but energy changes due to the RP oscillatory component may start earlier. This leads wider detection window which means earlier detection latency. Sensitivity (TPR) is defined as the percentage of correctly detected RMIs. The best performance of the proposed RP detection algorithm for each subject in terms of maximum TPR vs. minimum average number of FPs/min is determined from the knee point of the ROC curve (Fig. 7) from which the best coefficient "*c*" is also determined.

Experiments

Data

Three datasets were considered in this study: physionet (physionet-R03) movement dataset [29,30,31], BCI competition IV (BCICIV-1) imagery movement dataset [32,33] and our own dataset of voluntary left hand movements of pressing push buttons. The two datasets, physionet-R03 movement dataset of closing left and right fist and BCICIV-1 hand and foot imagery movement dataset, were recorded by giving visual cues to subjects for doing predefined real or imagery movements for predefined trials and rest at the end of each trial. The experimental setup for recording our own dataset of voluntary left hand movement has been described in the next section.

Experimental setup

Ten 25–35 year old subjects participated in the experiment. They were asked to sit relaxed and randomly move their left hands while pressing a soft push button in their hands to be marked as the movement onset. The push button pressing was validated by finding the time of crossing over 10% of local maximum amplitude of the related EMG signal. The average duration of each experiment was 5 min. No cues for starting a movement or rest were given in order to simulate a real-life scenario. They were only asked to rest at least 5 s after each movement. The experiments were repeated for subjects to help them be more relaxed and focused on their movement task without any movement imagination. The 64-electrode EEG signals were recorded with sampling frequency of 256 Hz and 64 EEG electrodes (10–20 standard electrode placement) of g.USBamp (g.tec) recording device at Iranian National Brain Mapping Laboratory (NBML) [34]. Ground and reference electrodes were attached to mastoid and nasion respectively. In this paper we only processed channel Cz for the reasons primarily explained.

Results

For the RP detection related to RMI, here the following quantification parameters are defined: If the mid-point of each final selected RP interval (In a pseudo online paradigm RPs are detected in the duration of negative ramp (slope1)) locates in a duration of −2 s to 200 ms around a movement onset, it is marked as TP, otherwise it is marked as FP. For each truly detected RP, latency is defined as the difference of RP detection time and movement onset. A negative latency means an early detection of RP. For BCICIV-1 and physionet-R03 datasets, those detected RP intervals which are overlapped with true RP events are marked as TPs. Those RPs detected in the rest intervals are marked as FPs. As the detection algorithm seeks for RPs, sensitivity (TPR) is defined as the percentage of all RP events correctly detected as RPs. The accuracy is defined as the percentage of correctly detected RPs (TPs) from all RPs detected by the algorithm. The average number of FPs/min is also reported for each subject. The quantitative parameters are defined by:

$$TPR\ (\%) = \frac{\textbf{\textit{Number of true RP detections (TPs)}}}{\textbf{\textit{Total number of RP events}}} \times 100 \tag{12}$$

$$Accuracy\ (\%) = \frac{\textbf{\textit{Number of true RP detections (TPs)}}}{\textbf{\textit{Total number of RP detections}}} \times 100 \tag{13}$$

$$Number\ of\ FPs \Big/ min = \frac{\textbf{\textit{Number of false RP detections (FPs)}}}{\textbf{\textit{Total rest duration in minutes}}} \tag{14}$$

We had an accuracy of 91.2±2.04%, a sensitivity of 81.1±5.23%, an average number of FPs/min of 1.6±0.69 and a negative latency of

Table 1
Quantitative results of RP detection for 3 datasets.

Subjects	Sensitivity (TPR) (%)			Number of FPs/min			Accuracy (%)			Latency (ms)	
	Our data (movement)	Physionet-R03 (movement)	BCICIV-1 (imagery)	Our data (movement)	Physionet (movement)	BCICIV-1 (imagery)	Our data (movement)	Physionet-R03 (movement)	BCICIV-1 (imagery)	Our data (movement)	Otherdata
S1	84	67	90	1	1	3	94	90	89	−250	-
S 2	82	93	96	2	3	1	90	85	93	−257	-
S 3	86	86	65	1	2	2	91	80	95	−48	-
S 4	82	73	90	2	4	1	88	80	88	−305	-
S 5	80	80	71	1	4	1	93	82	84	−27	-
S6	70	80	90	3	3	1	88	85	91	−786	-
S7	75	73	85	1	2	1	92	88	90	−518	-
S8	85	73		1	2		92	90		−705	-
S9	87	67		2	2		93	89		−707	-
S10	80	73		2	1		91	85		−534	
Mean	81.1	76.5	83.85	1.6	2.4	1.4	91.2	85.4	90	−384.9	
STD	5.23	8.27	11.42	0.69	1.07	0.7	2.04	3.83	3.56	296.5	

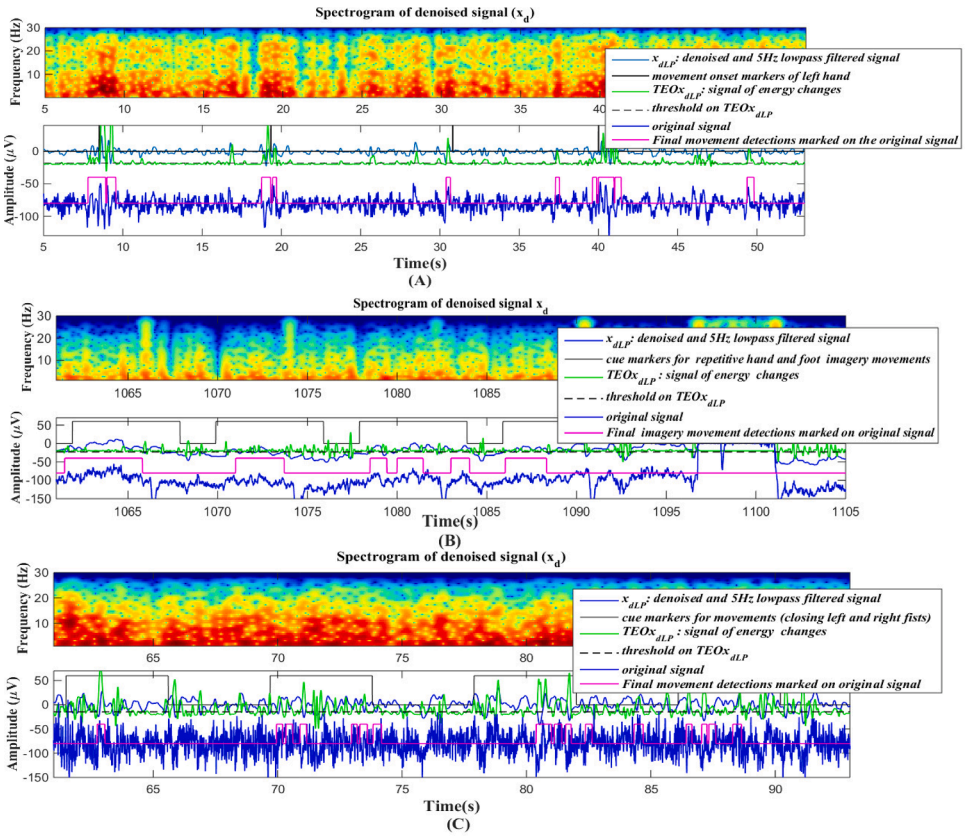

Fig. 8. (A) Detected RMIs for left hand (pressing push button) are shown by pink vertical bars on the original signal (Cz) from one healthy subject of our own dataset. Black vertical bars shown on the denoised and lowpass filtered signal (x_{dLP}) are the movement onsets. FPs are due to inevitable IMIs. (B) Detected hand and foot IMIs are shown by pink rectangles on the original signal (Cz) from one healthy subject of BCICIV-1 dataset [25]. Black rectangles shown on the denoised and lowpass filtered signal (x_{dLP}) are the cue durations for imagery movements. High amplitude blinkings which are obvious in the original signal have been well suppressed in x_{dLP}. (C) Detected RMIs for closing left and right fists are shown by pink rectangles on the original signal (Cz) from one healthy subject of physionet dataset [23]. Black rectangles shown on x_{dLP} are the movement cue durations.

−384.9±296.5 ms before the movement onsets using our own database. The proposed method was also evaluated on physionet-R03 movement dataset (closing left and right fist) [21-23] and BCICIV-1 imagery dataset (hand and foot) [24,25], with average signal duration of two minutes and thirty minutes for each subject respectively. We were not able to calculate the latency for physionet movement dataset due to lack of markers for the movement onsets. We had only visual cue onsets and cue durations for real and imagery movements. We achieved an accuracy of 90±3.56%, a sensitivity of 83.85±11.42%, an average number of FPs/min of 1.4±0.7 for detection of IMIs from the BCICIV-1 imagery dataset and an accuracy of 85.4±3.83%, a sensitivity of 76.5±8.27% and an average number of FPs/min of 2.4±1.07 for detection of RMIs from the physionet-R03 movement dataset. The quantitative results are depicted in Table 1. The results of automatic RP detection for one subject of each dataset are shown in Fig. 8.

Discussion

Here, a method for automatic, fast and accurate detection of movement intentions of different limbs has been developed for single channel EEG. Unlike the existing works which split the signals into windows or trials for pattern recognition or classification, our threshold-based method is applied to the whole signal on each 10 s non-overlapping signal length. The detection method is based on tracking energy changes of low frequency denoised signals. It takes 0.1 s on a corei5 system of 4GB RAM and 2 GHz CPU speed to process a 5-minute signal. Due to the simplicity of denoising and detection methods applied to single channel Cz, there is potential for online implementation on low cost movement neurofeedback devices for neuromodulation of neuromuscular interactions in stroke patients. Compared to a similar work with a statistical analysis approach applied to multiple channel EEG of hand movement in [35] which resulted in an average 96.37% accuracy and an average 77.93% sensitivity, our results led to lower accuracy (91.2%) but higher sensitivity (81.1%). Their achieved average onset prediction latency (−500 ms) was less than ours (−384.9 ms), i.e. they were earlier in RP detection. They didn't evaluate their method on imagery movements also didn't report the computation time of their method to compare with the speed of our proposed method. The validity of our detection method has been evaluated not only on our own hand movement dataset but also on two other well-known datasets: physionet-R03 hand movement [31] and BCICIV-1 hand and foot imagery movement datasets [33]. Quantitative results (Table 1) show that our detection method is capable of detecting both real and imagery movements with high accuracy. Our proposed method is faster and has a much better performance (an average accuracy of 91.2%, average number of FPs/min of 1.6 and sensitivity of 81.1%) than that in our previous work [17] based on template matching (an average FPR of 28.96% and sensitivity of 77.1%). In comparison with the results in [9] which used AR based features as input to an artificial neural network, we achieved the same accuracy but more average onset prediction latency (−384.9 ms) than theirs (−600 ms), i.e., they were earlier in detection of movement intention. Authors of [4] achieved an average classification accuracy of 87% for RMI detection vs. rest and an average classification accuracy of 73% for IMI detection vs. rest by applying their neural network classifier to spectral features from each 1 s window of source space signals on motor cortex. Our achieved accuracies are better than theirs, especially for discrimination of imageries vs. rest. Applying a combination of wavelet transform and SVM classifier to 8-channel EEG, authors in [11] predicted the gait intention of 6 healthy subjects in a pseudo online environment with an average accuracy of 88.23%, an average sensitivity of 85.42%, an average number of FPs/min of 6.8 and an average latency of −1002 ms. Their achieved latency is earlier than ours, but their detection algorithm results in more number of FPs/min than ours. In comparison with our threshold based eye blinking artefact rejection algorithm, their ICA based artefact rejection algorithm is not computationally efficient for their online preprocessing. Compared to

Table 2
Comparision of results from similar studies with present study in terms of average TPR (%), FPs/min (Specificity(%)), Accuracy (%), and Latency (ms).

Study	Method	Task (EEG electrodes)	TPR (%)	FPs/min(Specificity (%))	Accuracy (%)	Latency (ms)
Mirzaee et al. [35]	Statistical analysis	Cued hand movement (multiple)	77.93	(98.52)	96.37	−500
Nguyen et al. [9]	ANN	Breaking during driving (multiple)	88.4	(91.8)	91	−600
Ofner et al. [4]	ANN (source space)	upper limb movement (multiple)	–	–	87	–
Ofner et al. [4]	ANN (source space)	IMI of upper limb (multiple)	–	–	73	–
Hasan et al. [11]	SVM classifier	Voluntary gait (multiple)	85.42	6.8	88.23	−1002
Jochumsen et al. [16]	Template matching	Cued palmar grasp (single)	78	1.5	–	−150
Present study	proposed method	IMI of hand from BCICIV (single)	83.85	1.4	90	–
Present study	proposed method	Voluntary hand movement (single)	81.1	1.6	91.2	−384.9

Algorithm 1
EEG preprocessing steps.

Input signal: $\boldsymbol{x}$ (raw EEG data of Cz channel)

Step1: TVD, 1–30 Hz bandpass filtering and myogenic rejection by replacing each 2 s EEG segment with the amplitude exceeding 110 μV with zero-mean random numbers resulting in $\boldsymbol{x}_{TVD}$,

Step2: Threshold on $\boldsymbol{x}_{TVD}$ for blinking artefact detection and replacing 0.5 s around mid-point of each artefact contaminated segment with previous clean segment resulting in $\boldsymbol{x}_{d}$,

Step3: 5 Hz 4th order butterworth lowpass filter resulting in $\boldsymbol{x}_{dLP}$.

the template matching algorithm on single channel EEG in [16] which resulted in an average TPR of 78% and an average detection latency of −150 ms, our RMI detection on single channel EEG performed better (an average sensitivity of 81.1% and an average onset detection latency of −384.9 ms). The above mentioned studies aiming at accurate detection of RPs were not applied to BCICIV-1 [33] and Physionet-R03 [31] datasets. So, we were not able to compare our quantitative results on these datasets. Unfortunately, most papers on these datasets focus on feature selection and classification of different limb movements [36], which were not the objective of this study. Deep learning the denoised spectrogram images is the subject of our next study for classification of different limb movements. Implementation of our method on three datasets; we showed the generalization of our RP detection method for detection of the RPs related to any limb movement as shown in Fig. 8. Quantitative results in Table 1 validate the feasibility of our method for RP detection of different limbs. Table 2 shows an overview of similar studies for comparison.

From [1,2], for both RMI and IMI the brain generates RP, but the RP associated with RMI may be stronger with higher amplitudes in order to trigger a real movement. The reader is referred to Fig. 8 for visual comparison. Actually, the reason why we plotted Fig. 8 was not only to show the generalization of our RP detector performance for detection of RPs of different limbs from the three datasets, but also to show the RPs from RMI (Fig. 8(A) and (C)) and IMI (Fig. 8(B)) for comparison.

The equivalence between the RPs generated by RMI and IMI encourages recovery or neuromodulation of the stroke patients by imagery movements. These patients are trained to generate RPs by focusing on IMI of their paralyzed limb, inorder to control a prosthetic limb or activate an attached functional electric stimulation (FES) electrode. In fact, focusing on generating better RPs by their IMIs helps RP classifier software with higher classification accuracy, which means better synchronization between the patient and the control unit. Better synchronization gives the patient a sense of self paced voluntary movement. Upon this success, the patients are more encouraged to provide the classifier with better RPs by focusing on their IMIs. Over therapy sessions they restore the functionality of their paralyzed limb [37].

The advantage of our RP detector is that you can make changes to the $Threshold_{TEO_{x_{dLP}}}$ (in (9)) by changing the coefficient "c" or to the minimum duration constraint (which was 300 ms from our experiment, not the other datasets) and achieve higher sensitivities. But we used one criterion for quantitative analysis for all the datasets. Moreover, we didn't have onsets for RMIs of physionet datasets to calculate minimum durations of RPs.

Conclusion

In this work, which is applicable to BCI, we visually detected the RPs with a time-frequency based EEG analysis and automatically detected the RPs from the low frequency denoised single channel EEG with a fast threshold-based method using the nonlinear TEO and morphological properties of the RP waveform without any data splitting into trials. In conclusion, achieving an acceptable average RMI detection latency before movement execution (−384.9 ms), a high average detection accuracy (91.2%), an acceptable average sensitivity (83.85%) and an average low number of FPs/min (1.4) through a fast algorithm on a single electrode show the capability of our method to be integrated in real-time low cost neuromodulation and rehabilitation devices. It can also be integrated within entertaining rehabilitation tools used at home for monitoring recovery of the patients after stroke.

Declaration of Competing Interest

The authors declare no conflict of interest.

Acknowledgments

The first authors would like to thank the experiment participants for their collaboration and the reviewers for their constructive comments.

Supplementary materials

Supplementary material associated with this article can be found, in the online version, at doi:10.1016/j.cmpbup.2021.100027.

References

[1] H.H. Kornhuber, L. Deecke, Hirnpotentialänderungen beim Menschen vor und nach Willkürbewegungen und passiven Bewegungen des Menschen, dargestellt mit Magnetbandspeicherung und Rückwärtsanalyse, Pflügers Arch. Physiol. 281 (1964) 52, https://doi.org/10.1007/BF00412364, https://doi.org/.

[2] L. Deecke, H.H. Kornhuber, Human freedom, reasoned will, and the brain: the Bereitschafts potential story, in: M. Jahanshahi, M. Hallett (Eds.), The Bereitschafts potential. Movement related Cortical Potentials, Kluver Academic/Plenum, New York, 2003, pp. 283–320, https://doi.org/10.1007/978-1-4615-0189-3_17, https://doi.org/.

[3] H. Shibasaki, M. Hallett, What is the Bereitschaftspotential? Clin. Neurophysiol. 117 (2006) 2341–2356, https://doi.org/10.1016/j.clinph.2006.04.025, https://doi.org/.

[4] P. Ofner, A. Schwarz, J. Pereira, G.R. Müller-Putz, Upper limb movements can be decoded from the time-domain of low-frequency EEG, PLoS ONE 12 (2017), https://doi.org/10.5281/zenodo.834976 e0182578https://doi.org/.

[5] B. Blankertz, G. Curio, K.R. Müller, Classifying single trial EEG: towards brain computer interfacing, in: Proceedings of the 15th Annual Neural Information Processing Systems Conference, Vancouver, BC, Canada, 3-8 December 2001, pp. 157–164.

[6] R. Beisteiner, P. Höllinger, G. Lindinger, W. Lang, A. Berthoz, Mental representations of movements. Brain potentials associated with imagination of hand movements, Electroencephalogra. Clin. Neurophysiol./Evoked Potential. Sect. 96 (1995) 183–193, https://doi.org/10.1016/0168-5597(94)00226-5, https://doi.org/.

[7] S. Aliakbaryhosseinabadi, N. Jiang, A. Vuckovic, K. Dremstrup, D. Farina, N. Mrachacz-Kersting, Detection of movement intention from single-trial

movement-related cortical potentials using random and non-random paradigms, Brain-Comput. Interface. 2 (2015) 29–39, https://doi.org/10.1007/978-3-319-08072-7_42, https://doi.org/.
[8] S. Masaad, S. Jassim, L. Mahdi, Z. Bahri, Versatile brain-computer-interface for severely-disabled people, Int. J. Comput. Digit. Syst. 1 (2021) 463–471, https://doi.org/10.12785/ijcds/100145, https://doi.org/.
[9] T.H. Nguyen, W.Y. Chung, Detection of driver braking intention using EEG signals during simulated driving, Sensors 19 (2019) 2863, https://doi.org/10.3390/s19132863, https://doi.org/.
[10] O. Bai, V. Rathi, P. Lin, D. Huang, H. Battapady, D.Y. Fei, L. Schneider, E. Houdayer, X. Chen, M. Hallett, Prediction of human voluntary movement before it occurs, Clin. Neurophysiol. 122 (2011) 364–372, https://doi.org/10.1016/j.clinph.2010.07.010, https://doi.org/.
[11] S.S. Hasan, M.R. Siddiquee, O. Bai, Asynchronous Prediction of Human Gait Intention in a Pseudo Online Paradigm Using Wavelet Transform, IEEE Trans. Neural Syst. Rehab. Eng. 28 (2020) 1623–1635, https://doi.org/10.1109/TNSRE.2020.2998778, https://doi.org/.
[12] E.N. Kamavuako, M. Jochumsen, I.K. Niazi, K. Dremstrup, Comparison of features for movement prediction from single-trial movement-related cortical potentials in healthy subjects and stroke patients, Comput. Intel. Neurosc. 2015 (2015), https://doi.org/10.1155/2015/858015 https://doi.org/.
[13] I.K. Niazi, N. Jiang, O. Tiberghien, J.F. Nielsen, K. Dremstrup, D. Farina, Detection of movement intention from single-trial movement-related cortical potentials, J. Neural Eng. 8 (2011), https://doi.org/10.1080/2326263X.2015.1053301, 066009https://doi.org/.
[14] P. Ahmadian, S. Cagnoni, L. Ascari, How capable is non-invasive EEG data of predicting the next movement? A mini review, Front. Hum. Neurosci. 7 (2013) 124, https://doi.org/10.3389/fnhum.2013.00124, https://doi.org/.
[15] P. Ahmadian, S. Sanei, L. Ascari, L. González-Villanueva, M.A. Umiltà, Constrained blind source extraction of readiness potentials from EEG, IEEE Trans. Neural Syst. Rehab. Eng. 21 (2012) 567–575, https://doi.org/10.1109/TNSRE.2012.2227278, https://doi.org/.
[16] M. Jochumsen, I.K. Niazi, H. Rovsing, C. Rovsing, G.A. Nielsen, T.K. Andersen, N. P. Dong, M.E. Sørensen, N. Mrachacz-Kersting, N. Jiang, D. Farina, Detection of movement intentions through a single channel of electroencephalography. Replace, Repair, Restore, Relieve–Bridging Clin. Eng. Sol. Neurorehab., Springer, Cham, 2014, pp. 465–472, https://doi.org/10.1007/978-3-319-08072-7_69, https://doi.org/.
[17] M. Mahmoodi, B.M. Abadi, H. Khajepur, M.H. Harirchian, A robust beamforming approach for early detection of readiness potential with application to brain-computer interface systems, in: 2017 39th Annual International Conference of the IEEE Engineering in Medicine and Biology Society (EMBC), Jeju Island, South Korea, Jul. 2017, pp. 2980–2983, https://doi.org/10.1109/EMBC.2017.8037483, https://doi.org/.
[18] K. Sekihara, S.S. Nagarajan, Adaptive Spatial Filters For Electromagnetic Brain Imaging, Springer Science & Business Media, May. 2008, https://doi.org/10.1007/s11277-017-4953-1 https://doi.org/.
[19] S. Amin-Nejad, T.A. Gashteroodkhani, K. Basharkhah, A comparison of MVDR and LCMV beamformers' floating point implementations on FPGAs, Wirel. Pers. Commun. 98 (2018) 1913–1929, https://doi.org/10.1007/s11277-017-4953-1, https://doi.org/.
[20] S. Amin-Nejad, K. Basharkhah, T.A. Gashteroodkhani, Floating point versus fixed point tradeoffs in FPGA Implementations of QR Decomposition Algorithm, Eur. J. Electr. Eng. 3 (2019), https://doi.org/10.24018/ejece.2019.3.5.127 https://doi.org/.
[21] S. Solnik, P. DeVita, P. Rider, B. Long, T. Hortobágyi, Teager–Kaiser Operator improves the accuracy of EMG onset detection independent of signal-to-noise ratio, Acta. Bioeng. Biomech./Wroclaw Univ. Technol. 10 (2008) 65, https://doi.org/10.1007/s00421-010-1521-8, https://doi.org/.
[22] L. Condat, A direct algorithm for 1-D total variation denoising, IEEE Signal Process. Lett. 20 (2013) 1054–1057, https://doi.org/10.1109/LSP.2013.2278339, https://doi.org/.
[23] L.I. Rudin, S. Osher, E. Fatemi, Nonlinear total variation based noise removal algorithms, Phys. D 60 (1992) 259–268, https://doi.org/10.1016/0167-2789(92)90242-F, https://doi.org/.
[24] M.A. Figueiredo, J.B. Dias, J.P. Oliveira, R.D. Nowak, On total variation denoising: a new majorization-minimization algorithm and an experimental comparisonwith wavalet denoising, in: Proceedings of the IEEE International Conference on Image Processing, IEEE, Atlanta, GA, USA, Oct. 2006, pp. 2633–2636, https://doi.org/10.1109/ICIP.2006.313050, https://doi.org/.
[25] I. Selesnick, Total Variation Denoising (an MM algorithm), NYU Polytechnic School of Eng. Lecture Notes, New York, NY, USA, Sep. 2012.
[26] I. Selesnick, I. Bayram, Total variation filtering, Tech. Rep (2010).
[27] I. Selesnick, Generalized total variation: tying the knots, IEEE Signal Process. Lett. 22 (2015) 2009–2013, https://doi.org/10.1109/LSP.2015.2449297, https://doi.org/.
[28] J.F. Kaiser, On a simple algorithm to calculate the 'energy' of a signal, in: Proceedings of the IEEE International Conference on Acoustics, Speech, and Signal Processing, IEEE, Albuquerque, NM, USA, 1990, pp. 381–384, https://doi.org/10.1109/ICASSP.1990.115702, 3–6 Apr.https://doi.org/, doi:.
[29] G. Schalk, D.J. McFarland, T. Hinterberger, N. Birbaumer, J.R. Wolpaw, BCI2000: a general-purpose brain-computer interface (BCI) system, IEEE Trans. Biomed. Eng. 51 (2004) 1034–1043, https://doi.org/10.1109/TBME.2004.827072, https://doi.org/.
[30] A.L. Goldberger, L.A. Amaral, L. Glass, J.M. Hausdorff, P.C. Ivanov, R.G. Mark, J. E. Mietus, G.B. Moody, C.K. Peng, H.E. Stanley, PhysioBank, PhysioToolkit, and PhysioNet: components of a new research resource for complex physiologic signals, Circulation 101 (2000) 215–220, https://doi.org/10.1161/01.cir.101.23.e215, https://doi.org/.
[31] Physionet EEG motor movement dataset. https://doi.org/ 10.13026/C28G6P, 2020 (Accessed 15 November 2020).
[32] B. Blankertz, G. Dornhege, M. Krauledat, K.R. Müller, G. Curio, The non-invasive Berlin brain–computer interface: fast acquisition of effective performance in untrained subjects, Neuroimage 37 (2007) 539–550, https://doi.org/10.1016/j.neuroimage.2007.01.051, https://doi.org/.
[33] BCI competition IV imagery dataset. http://www.bbci.de/competition/iv/.
[34] National brain mapping laboratory. http://nbml.ir/FA/services/EEG-Lab, 2020 (Accessed 15 November 2020).
[35] M.S. Mirzaee, S. Moghimi, Detection of reaching intention using EEG signals and nonlinear dynamic system identification, Comput. Meth. Prog. Bio. 175 (2019) 151–161, https://doi.org/10.1016/j.cmpb.2019.04.023, https://doi.org/.
[36] M. Dai, D. Zheng, R. Na, S. Wang, S. Zhang, EEG Classification of Motor Imagery Using a Novel Deep Learning Framework, Sensors 19 (2019) 551, https://doi.org/10.3390/s19030551, https://doi.org/.
[37] Recoverix, the revolutionary stroke therapy by g.tec. https://www.recoverix.at/.